JOURNAL OF MATERIALS SCIENCE 32 (1997) 4865–4874

Transformation toughening in the γ-TiAl–β-Ti–V system

Part I *Finite element analysis of a crack touching the interface*

M. GRUJICIC, P. DANG
Program in Materials Science and Engineering, Department of Mechanical Engineering, 241 Flour Daniel Building, Clemson University, Clemson, SC 29634–0921, USA

Atomistic simulation of transformation toughening due to martensitic transformation in Ti–V phase particles dispersed in a γ-TiAl matrix containing cracks requires knowledge of the continuum elastic stress and displacement fields for the problem of a crack touching the γ–β interface. Because of the anisotropic characters of the two phases, analytical solutions for these fields are not available and they must be determined numerically. In the present paper a finite element method-based eigenanalysis is developed and subsequently applied to the γ–β system to determine the order of the stress singularity and the angular dependences of the stress and displacement fields. These fields are subsequently used to enrich the finite elements surrounding the crack tip and, through the use of the general finite element code ABAQUS, to determine the generalized stress intensity factors and thus the total singular crack-tip stress and displacement fields. It is found that there are two coupled singular terms in the singular stress and displacement fields, and consequently pure (uniaxial) mode I loading gives rise to mixed modes I–II near-crack-tip behaviour.

1. Introduction

γ-TiAl is one of the candidate materials for high temperature applications because of its attractive high temperature mechanical properties, low density and good oxidation resistance. Currently, however, wide scale application of this material is limited due to its inferior tensile ductility and toughness at temperatures below $\sim 600\,^{\circ}C$. Various approaches have been utilized, with modest success, in order to resolve this problem. For instance: alloying is used to reduce tetragonality of the TiAl unit cell [1], and ceramic fibres and whiskers embedded in the γ-TiAl matrix to refine slip length [2], etc. Recently, we found that the use of metastable Ti–V–base body centred cubic (b.c.c.) β-phase inclusions that can undergo a stress–strain induced martensitic transformation can double fracture toughness of single-phase γ-TiAl [3]. Microstructural analysis of partially fractured specimens of γ–β alloys shows that cracks preferentially form and grow in the γ-TiAl matrix and that stress–strain induced martensitic transformation in the β particles ahead of the advancing crack tip is the dominant toughening mechanism. It should be noted that similar dispersed-phase transformation toughening effects have been previously observed in high-strength steels [4] and ceramics [5], and they are responsible for the record fracture toughness levels achieved in these materials.

Modelling of dispersed phase transformation toughening is traditionally done using a continuum approach and phenomenological constitutive relations of materials [6]. These models, however, fail to include short range interactions between the cracks and the dispersed particles. Because these interactions make major contributions to transformation toughening, continuum-based models have only limited capabilities in elucidating the evolution of materials in the region in front of the advancing crack and in predicting the associated increase in toughness.

In the present two part paper, the interaction of a crack in a γ-TiAl matrix with a β-Ti–V particle at a crack tip is analysed using molecular dynamics atomistic simulations. Our current computational capabilities allow us to carry out such simulations using a computation crystal containing only several thousand atoms. Such an atomistic computational crystal can be considered too small to represent the entire physical system of interest and this problem can be resolved by embedding the atomistic computational crystal into a larger continuum crystal. This is typically done by replacing the effect of the continuum crystal on the atomistic one, with a set of forces or displacements acting on the outermost atoms in the atomistic crystal. These forces and displacements (the boundary conditions) are obtained by solving the associated continuum problem. Specifically, for the case at hand, the boundary conditions require a knowledge of the displacement and stress fields for the case of a crack in a γ-TiAl matrix touching the γ–β interface. Because the two materials are anisotropic, analytical

0022–2461

solutions for the stress and displacement fields are not available and have to be determined numerically. Numerical derivation of the displacement and stress fields, through the use of a finite element method, is presented in Part 1 of this paper. Part 2 deals with molecular dynamics atomistic simulations of the evolution of materials associated with the martensitic transformation in a β particle in front of the crack tip and the resulting toughness enhancement.

The organization of this part is as following: In Section 2.1, detailed derivation and application to the γ-TiAl–β–Ti–V system of a finite element procedure for the calculation of the order of stress singularity and angular variations of the stress and displacement fields as presented. The procedure used to compute the generalized stress intensity factors, and in turn, determine the complete stress and displacement fields is discussed in Section 2.2. The concluding remarks are given in Section 3.

2. Discussion

2.1. Finite element derivation of singular stress and displacement fields

2.1.1. General consideration

The problem of a crack touching the interface is a specific example of the whole class of problems associated with the existence of a singular point (the point where stresses become infinite in magnitude) in multi-material wedges and junctions. For isotropic materials and for many cases of orthotropic materials, analytical solutions for the order of the stress singularity and for angular variations of the stress and displacement fields around a singular point have been derived [7–12]. These solutions are next used to enrich the stiffness matrix of the finite elements surrounding a singular point and in conjunction with the standard elements to account for specific far-field (specimen) geometry and loading conditions [13, 14]. This procedure yields the stress intensity factors for each of the singular terms of the stress and displacement fields and, in turn, the total singular stress and displacement fields.

When analytical solutions are not available for a given combination of materials and/or for a given type of geometrical discontinuity, as is the present case, the finite element method can be used to numerically determine the order of the stress singularity and the angular variations of the stress and displacement fields in the vicinity of a singular point (crack tip). There are a number of such finite formulations, some include direct curve fitting of the computed stress [15], frequently combined with an iterative procedure to obtain the convergence of the order of stress singularity [16]. An alternative finite element formulation is the eigenanalysis introduced by Bazant and Estenssoro [17] and Yamada and Okumura [18], which allows direct determination of the order of the stress singularity and the angular variations of the stress and displacement fields. The validity of the eigenanalysis method was verified in [17] and [18] by applying it to the problem of a mode I crack meeting the surface in an isotropic material and it was shown to yield results that were in excellent agreement with the analytical solutions for this problem derived by Benthem [19].

The problem that is analysed in the present paper is depicted in Fig. 1a. A crack in a γ-matrix has propagated under the influence of mode I loading until its tip has made contact with a β-phase particle. A close-up view of the crack-tip region is shown in Fig. 1b. The objective of the present paper is to develop a numerical procedure for calculating the displacements and the stresses acting on the outer boundary of the close-up region shown in Fig. 1b. To simplify the procedure the region was assumed to be infinite in the z-direction and also that the components of strain in the same direction were zero (the plane strain condition). This considerably simplified the analysis of the problem at hand by allowing it to be treated as a two-dimensional problem.

According to Munz and Yang [20], the stress field for a two-dimensional problem of a crack touching on interface in a bi-material can be expressed as a sum of terms each in the form

$$\sigma_{ijk}(r, \theta) = \frac{K_k}{r^{1-\lambda_k}} h_{ijk}(\theta) \quad i, j = r, \theta \;\; k = 1, 2, \ldots, N \quad (1)$$

where the indices i and j are used to represent the stresses σ_{rr}, $\sigma_{r\theta}$ and $\sigma_{\theta\theta}$: r and θ are the polar coordinates; K is the "generalized" stress intensity factor; λ_k the order of the stress singularity; and $h_{ijk}(\theta)$ the angular stress function associated with the kth singular term. Equation 1 shows that the stress field is singular at the crack tip ($r = 0$) for each real λ_k less than one. In addition, to satisfy the condition for finiteness of the strain energy, admissible values of λ should satisfy the condition $\lambda > 0$. In general one finds for a bi-material problem two or more values of λ that satisfy the condition $0 < \lambda < 1$ and hence, the total singular part of the stress field is obtained as the sum of $\sigma_{ijk}(r, \theta)$ given by Equation 1 over all such values of λ_k.

The radial and tangential displacement fields u_{rk} and $u_{\theta k}$, are also given by Munz and Yang [20] as

$$u_{ik}(r, \theta) = K r^{\lambda} f_{ik}(\theta) \quad i = r, \theta \quad k = 1, 2 \qquad (2)$$

where $f_{ik}(\theta)$ is the angular displacement function, and the "singular" portion of the displacement is obtained

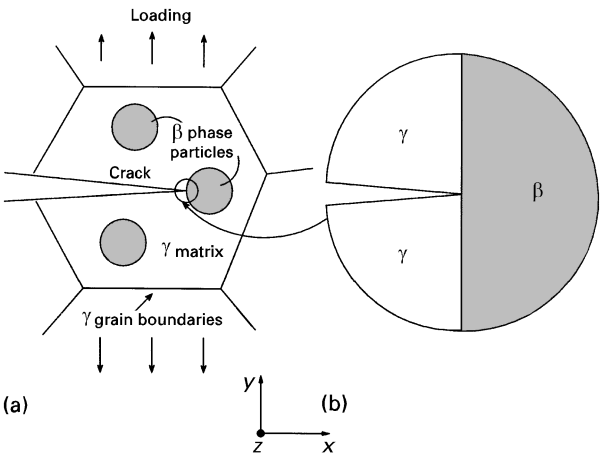

Figure 1 (a) A crack in the γ matrix impinging on a β-phase particle and (b) a close-up view of the crack-tip region.

by a summation over all λ_k which satisfy the condition $0 < \lambda < 1$.

As will be shown in this section, the stress singularity and the angular dependences of the stress and displacement fields, i.e. the $h_{ijk}(\theta)$ and $f_{ik}(\theta)$ functions, can be obtained by imposing the near-field stress, and displacement boundary and continuity conditions on the boundaries and interfaces of the bi-crystal shown in Fig. 1b. The stress and displacements are then determined to within multiplicative constants, the generalized stress intensity factors K (one for each admissible value of $0 < \lambda < 1$). Evaluation of the generalized stress intensity factors is carried out in the next section through the analysis of a global problem that takes into account the geometry of the specimen and the externally applied loading conditions.

The stress and the displacement fields for the problem at hand are determined using an eigenfunction finite element formulation analogous to the one for the inplane loading of anisotropic materials containing geometric discontinuities as originally proposed by Yamada and Okumura [18]. When the order of the stress singularity is real, obtaining the stress and displacement fields from the formulation of Yamada and Okumura is straightforward as will be shown here.

Fig. 2 shows a crack touching the interface in a bimaterial crystal where the stress singularity occurs at the crack tip, O. In order to determine the order of the stress singularity, λ, and the angular variation of the stress and displacement fields, the region surrounding the crack tip is divided into several quadratic sector elements, where the location of each element is defined in polar co-ordinates by its nodes 1–3. The location of a point, P, in the element can then be defined using the following singular transformation [21]

$$r = r_0\left(\frac{1+\xi}{2}\right)^{1/\lambda} \quad \text{or} \quad \varrho = \frac{r}{r_0} = \left(\frac{1+\xi}{2}\right)^{1/\lambda} \tag{3}$$

and

$$\theta = \sum_{i=1}^{3} H_i\theta_i \tag{4}$$

where

$$H_1 = \tfrac{1}{2}(-\eta + \eta^2), \quad H_2 = 1 - \eta^2, \quad H_3 = \tfrac{1}{2}(\eta + \eta^2) \tag{5}$$

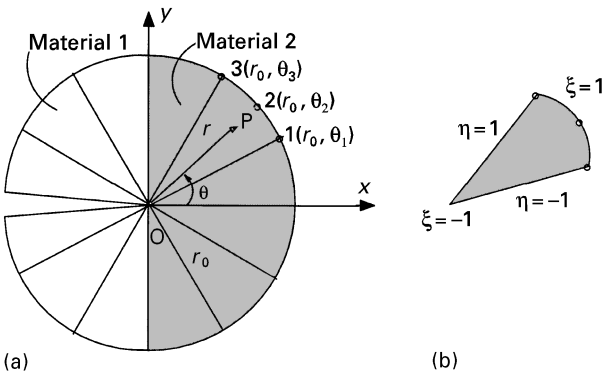

Figure 2 Definition of (a) element geometry and (b) the natural co-ordinates in a typical structure where a singular stress state occurs.

and η and ξ are natural co-ordinates of the elements as defined in Fig. 2.

In accordance with Equation 2, the displacement field in the element relative to the inplane displacement of the crack tip, $\bar{u}$, due to inplane loads is assumed to have the following form

$$\bar{u} = \varrho^{\lambda}\sum_{i=1}^{3}[H_i]\{\bar{u}_i\} = \varrho^{\lambda}[H]\{\bar{u}\} \tag{6}$$

where

$$[H_i] = \begin{bmatrix} H_i & 0 \\ 0 & H_i \end{bmatrix}$$

$\{\bar{u}_i\}^T = \{\bar{u}_{ri}\bar{u}_{\theta i}\}$ the inplane displacement vector of the node i ($i = 1, 2, 3$)

$$[H] = \begin{bmatrix} H_1 & 0 & H_2 & 0 & H_3 & 0 \\ 0 & H_1 & 0 & H_2 & 0 & H_3 \end{bmatrix}$$

and

$$\{\bar{u}\}^T = \{\bar{u}_{r1}\ \bar{u}_{\theta 1}\ \bar{u}_{r2}\ \bar{u}_{\theta 2}\ \bar{u}_{r3}\ \bar{u}_{\theta 3}\}$$

The strains are next obtained from proper differentiation of the displacements, which through the use of Equations 3–6 results in

$$\{\varepsilon\} = \begin{Bmatrix} \varepsilon_r \\ \varepsilon_\theta \\ \gamma_{r\theta} \end{Bmatrix} = \sum_{i=1}^{3}[B_i]\{\bar{u}_i\} = [B]\{\bar{u}\} \tag{7}$$

where

$$[B] = \frac{1}{r_0}\varrho^{\lambda-1}(\lambda[B_a] + [B_b])$$

$$[B_{ia}] = \begin{bmatrix} H_i & 0 \\ 0 & 0 \\ 0 & H_i \end{bmatrix}$$

$$[B_{ib}] = \begin{bmatrix} 0 & 0 \\ H_i & \dfrac{2}{\theta_S}\dfrac{\partial H_i}{\partial \eta} \\ \dfrac{2}{\theta_S}\dfrac{\partial H_i}{\partial \eta} & -H_i \end{bmatrix} \qquad i = 1, 2, 3 \tag{8}$$

During the derivation of $[B_{ib}]$ in Equation 8 it was assumed that $\theta_2 = (\theta_1 + \theta_3)/2$ and $\theta_S = \theta_3 - \theta_1$, and hence $\partial\eta/\partial\theta = 2/\theta_S$.

According to Equations 7 and 8 the strains, and hence the stresses are proportional to $\varrho^{\lambda-1}$ and thus any λ less than one gives rise to a singular stress at the crack tip. As discussed earlier the physically admissible values of λ must be greater than zero in order to satisfy the condition for finiteness of the strain energy and hence the admissible singular values of λ are in the range $0 < \lambda < 1$.

For each of the sector elements depicted in Fig. 2 to be in equilibrium they must satisfy the principle of virtual work, which for the plane strain case can be expressed as

$$\int_0^{r_0}\int_{\theta_1}^{\theta_3}(\sigma_r\delta\varepsilon_r + \sigma_\theta\delta\varepsilon_\theta + \tau_{r\theta}\delta\gamma_{r\theta})t\,r\,\mathrm{d}r\,\mathrm{d}\theta = r_0\int_{\theta_1}^{\theta_3}(T_r\delta\bar{u}_{r0} + T_{r\theta}\delta\bar{u}_{\theta 0})t\,\mathrm{d}\theta \tag{9}$$

where δu and $\delta\varepsilon$ are the virtual displacements and the corresponding virtual strains; T_r and $T_{r\theta}$ represent, respectively, the applied normal and shear stresses at the outer boundary of the element; $\bar{u}_{r0}$ and $\bar{u}_{\theta 0}$, the surface displacements at $r = r_0$; and t is the thickness of the element. It should be noted here that traction on the O1 and O3 element edges are not included in Equation 9 because these edges are either the internal edges in the material or they are stress-free crack faces.

Using the relations given in Equations 3–5, Equation 9 can be transformed into

$$\int_{-1}^{1}\int_{0}^{1}\frac{r_0^2\theta_s}{2}(\sigma_r\delta\varepsilon_r+\sigma_\theta\delta\varepsilon_\theta+\tau_{r\theta}\delta\gamma_{r\theta})\,t\varrho\,d\varrho\,d\eta = r_0\int_{-1}^{1}(T_r\delta\bar{u}_{r0}+T_{r\theta}\delta\bar{u}_{\theta 0})\,t\,d\eta \tag{10}$$

On the element surface $r = r_0$ and $\varrho = 1$ and in accordance with Equation 6

$$\delta\bar{u}_{r0}=\left[\sum_{i=1}^{3}H_i\delta\bar{u}_{ri}\right],\quad \delta\bar{u}_{\theta 0}=\left[\sum_{i=1}^{3}H_i\delta\bar{u}_{\theta i}\right] \tag{11}$$

or

$$\delta\{\bar{u}_0\}=[H]\delta\{\bar{u}\},\quad \delta\{\bar{u}_0\}^T=\delta\{\bar{u}_{r0}\bar{u}_{\theta 0}\}$$

Taking into account that $T_r = \sigma_{r0} = \sigma_r(r = r_0)$ and $T_{r\theta 0} = \tau_{r\theta}$ $(r = r_0)$, Equation 11 can then be transformed into

$$\int_{-1}^{1}\int_{0}^{1}\frac{r_0^2\theta_S}{2}(\delta\{\varepsilon\}\{\sigma\})\,t\varrho\,d\varrho\,d\eta = \frac{r_0\theta_S}{2}\int_{-1}^{1}\delta\{\bar{u}\}[H]^T\{\sigma_0\}\,t\,d\eta \tag{12}$$

where $\{\sigma\}^T=\{\sigma_r\sigma_\theta\tau_{r\theta}\}$ and $\{\sigma_0\}^T=\{\sigma_{r0}\tau_{r\theta 0}\}$.

Using Equations 7 and 8 and the material's constitutive relation $\{\sigma\}=[D]\{\varepsilon\}$, where $[D]$ is the stiffness matrix of the material, Equation 12 after integration of its left-hand side with respect to ϱ becomes

$$\frac{\theta_S t}{4\lambda}\delta\{\bar{u}\}^T\int_{-1}^{1}(\lambda[B_a]^T+[B_b]^T)[D](\lambda[B_a]+[B_b])\,d\eta\,\{\bar{u}\} = \frac{t\theta_S}{4\lambda}\delta(\bar{u}\}^T\int_{-1}^{1}[H][d](\lambda[B_a]+[B_b])\,d\eta\,\{\bar{u}\} \tag{13}$$

The stiffness matrix of the material is given as

$$[D]=\begin{bmatrix}D_{11}&D_{12}&D_{16}\\D_{11}&D_{22}&D_{26}\\D_{16}&D_{26}&D_{66}\end{bmatrix}$$

and

$$[d]=\begin{bmatrix}D_{11}&D_{12}&D_{16}\\D_{16}&D_{26}&D_{66}\end{bmatrix}$$

is comprised of the first row of the last row of the matrix $[D]$.

Equation 13 must hold for an arbitrary variation in nodal displacement, $\delta\{u\}$, and hence the $\delta\{u\}^T$ term can be eliminated from this equation, which when written for the entire domain S (i.e. for all the elements) becomes

$$(\lambda^2[A]+\lambda[B]+[C])\{\bar{U}\}=0 \tag{14}$$

where

$$[A]=\sum_S([k_a]-[k_{Sa}]) \tag{15}$$

$$[B]=\sum_S([k_b]-[k_{Sb}]) \tag{16}$$

$$[C]=\sum_S[k_c] \tag{17}$$

$$\{\bar{U}\}=\sum_S\{\bar{u}\} \tag{18}$$

$$[k_a]=\int_{-1}^{1}[B_a]^T[D][B_a]\,d\eta \tag{19}$$

$$[k_c]=\int_{-1}^{1}[B_b]^T[D][B_b]\,d\eta \tag{20}$$

Summation over S in Equations 15–18 implies assembly of the elements into a global model. For instance $\{\bar{U}\}=\{\bar{u}_{r1}\bar{u}_{\theta 1},\ \ldots,\bar{u}_{r,\,2n+1}\bar{u}_{\theta,\,2n+1}\}$, where n is the number of sector elements and hence $2n+1$ is the number of nodes.

$$[k_b]=\int_{-1}^{1}([B_a]^T[D][B_b]+[B_b]^T[D][B_a])\,d\eta \tag{21}$$

$$[k_{Sa}]=2\int_{-1}^{1}[H]^T[d][B_a]\,d\eta \tag{22}$$

and

$$[k_{Sb}]=2\int_{-1}^{1}[H]^T[d][B_b]\,d\eta \tag{23}$$

By inspection of the integrand in Equation 20, it can be established that matrix $[C]$ is singular, and consequently the characteristic Equation 14 can be transformed uniquely into the standard eigenvalue problem

$$[S]\begin{Bmatrix}\bar{V}\\\bar{U}\end{Bmatrix}=\lambda\begin{Bmatrix}\bar{V}\\\bar{U}\end{Bmatrix} \tag{24}$$

where

$$[S]=\begin{bmatrix}0&I\\-A^{-1}C&-A^{-1}B\end{bmatrix},\quad \{\bar{U}\}=\lambda\{\bar{V}\}$$

and

$$\begin{Bmatrix}\bar{U}\\\bar{V}\end{Bmatrix}^T=\{\bar{V}_{r1},\bar{V}_{\theta 1},\ \ldots,\bar{V}_{r,2n+1},\bar{V}_{\theta,\,2n+1},\bar{u}_{r1},\ \bar{u}_{\theta 1},\ \ldots,\bar{u}_{r,\,2n+1},\bar{u}_{\theta,\,2n+1}\}$$

The admissible values for the order of the stress singularity are obtained as eigenvalues, λ, in Equation 24 that satisfy the condition $0<\lambda<1$ and the corresponding nodal displacements, $\{U\}$, from the eigenvectors $\{\bar{V}/\bar{U}\}$ associated with each admissible value of λ.

The element matrices $[k_a]$, $[k_{Sa}]$, etc. in Equations 15–23 can be computed using Gaussian quadrature numerical integration procedure with the stiffness matrix of the material $[D]$ and $[d]$ being evaluated at each Gauss point. For the inplane behaviour to be decoupled from the antiplane behaviour, as was postulated here, the two anisotropic materials analysed must be symmetric with respect to the $z = 0$ plane, i.e. they must be at least monoclinically symmetric relative to this plane. When the two materials do not satisfy this symmetry condition, as will be shown is the

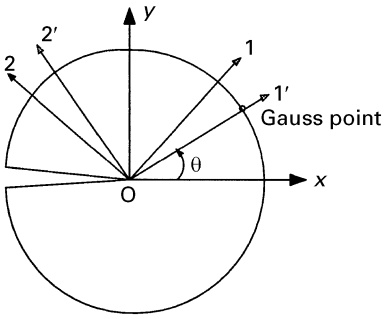

Figure 3 Reference co-ordinate systems used in the present study: x–y are global axes in the model, 1–2 are principal axes of the material's orthotropy, and 1′–2′ are local axes associated with a Gauss point.

present case, the inplane behaviour can still be separated from the antiplane behaviour provided the plane strain condition is imposed.

For the plane strain case, the stiffness matrix at a Gaussian point, whose polar axes 1′–2′ form an angle, θ, relative to the global x–y co-ordinate system (as indicated in Fig. 3) is defined as

$$[D] = [A]^{-1} = \begin{bmatrix} a_{11} & a_{12} & a_{16} \\ a_{11} & a_{22} & a_{26} \\ a_{16} & a_{26} & a_{66} \end{bmatrix}^{-1} \tag{25}$$

where

$$a_{11} = \frac{S_{11}S_{33} - S_{13}^2}{S_{33}},\ a_{12} = a_{21} = \frac{S_{12}S_{33} - S_{13}S_{23}}{S_{33}}$$

$$a_{22} = \frac{S_{22}S_{33} - S_{23}^2}{S_{33}},\ a_{16} = a_{61} = \frac{S_{16}S_{33} - S_{13}S_{36}}{S_{33}}$$

$$a_{66} = \frac{S_{66}S_{33} - S_{36}^2}{S_{33}},\ a_{26} = a_{62} = \frac{S_{26}S_{33} - S_{13}S_{36}}{S_{33}} \tag{26}$$

and S_{ij} represents the elements of the compliance matrix of the material, $[S]$, which is the inverse of the material's elastic constants matrix, $[D]$.

The material's elastic constants matrix is generally given in the 1–2 principal co-ordinate system of material's orthotropy (see Fig. 3) and hence before evaluating $[D]$ using Equation 25 one must transform $[C]$ into the local 1′–2′ co-ordinate system for a given Gauss point. This transformation is straightforward and involves the use of two rotation matrices, one relating the 1–2 and the x–y co-ordinate systems and the other relating the x–y and the 1′–2′ co-ordinate systems.

When the eigenvalue λ obtained by solving Equation 24 is real, the eigenvector $\{\bar{U}\}$ defines the relative inplane displacement at the nodes of these elements where $r = r_0$. Because these displacements are the same within a constant $(r/r_0)^{\lambda}$ for any r, the r and θ-components of the eigenvector $\{\bar{U}\}$ can be used to determine the angular variation of these components of the nodal displacements and in turn the use of a curve fitting procedure the angular displacement functions, $f_{ik}(\theta)$, Equation 2. The complete displacement field can then be written as

$$u_i = \sum_{j=1}^{n} K_j r^{\lambda_j} f_{ij}(\theta) \quad i = r, \theta \tag{27}$$

where n is the number of admissible eigenvalues, and K_j the generalized stress intensity factor corresponding to the admissible order of the stress singularity, λ_j.

Knowledge of the nodal displacements, $\{\bar{U}\}$, allows through the use of Equations 7 and 8, the determination of the strains. The stresses and their angular variations can next be determined from the strains by making use of the consecutive relation $\{\sigma\} = [D]\{\varepsilon\}$.

The procedure described in this section can be used when the admissible orders of the stress singularity are real. When the eigenvalues, λ, are complex, the eigenanalysis is more complicated [7]. Because complex λs were not found in the present work, this case will not be considered here.

2.1.2. Application to the γ-TiAl–β-Ti–V case

The procedure developed in the previous section is next used to determine the order of stress singularity and the angular variations of the stress and displacement fields in the γ-TiAl–β-Ti–V system. In accordance with the bi-material model shown in Fig. 2, γ-TiAl is defined as material 1 while β-Ti–V represents material 2.

In its principal co-ordinate system of material's orthotropy, the γ-phase, which has a face centred tetragonal structure, has six non-zero independent elastic constants: $C_{11} = 2.28$, $C_{12} = 1.02$, $C_{13} = 1.36$, $C_{33} = 2.78$, $C_{44} = 1.4$ and $C_{66} = 0.776$ (all in $10^{11}\ \mathrm{N\,m^{-2}}$) [3]. The β-phase has a body centred cubic structure and thus only three independent elastic constants [3]: $C_{11} = 1.121$, $C_{12} = 0.771$ and $C_{44} = 0.885$ ($10^{11}\ \mathrm{N\,m^{-2}}$) [3]. As will be discussed in Part 2 of this paper [22], the γ–β interface analysed is taken to be parallel to the closed packed planes in the two materials and accordingly the microscopic x–y–z co-ordinate system in Fig. 3, has the following relations to the crystallographic orientation of the two materials

$$x \parallel [1\,1\,1]_{\gamma} \parallel [\bar{1}\,1\,0]_{\beta}$$

$$y \parallel [0\,\bar{1}\,1]_{\gamma} \parallel [0\,0\,1]_{\beta}$$

$$z \parallel [2\,\bar{1}\,\bar{1}]_{\gamma} \parallel [1\,1\,0]_{\beta}$$

As explained earlier, the elastic stiffness matrices in the x–y–z co-ordinate systems can be readily obtained through the use of appropriate rotation matrices relating this co-ordinate system with the principal co-ordinate systems in the two structures.

The eigenvalue Equation 24 was found in the present case to yield two values of λ in the range $0 < \lambda < 1$. These values are shown in Table I. The accuracy of the solutions obtained is primarily affected by two factors: (a) the number of sector elements in the model and (b) the number of Gauss points used during the evaluation of the element's stiffness matrices. The former effect is due to the finite element discretization of the region studied, while the latter effect stems from the fact that due to the anisotropic

TABLE I The orders of the stress singularity, λ, for the γ-TiAl/β-Ti–V case

No. of elements in the model	Mode A			Mode B		
	No. of Gauss points			No. of Gauss points		
	3	4	5	3	4	5
4	–	–	0.506 30	–	–	0.464 20
8	–	–	0.479 11	–	–	0.426 30
16	0.480 85	0.479 34	0.478 87	0.413 32	0.412 33	0.411 50
20	0.480 97	0.479 05	0.478 85	0.412 91	0.412 30	0.411 38

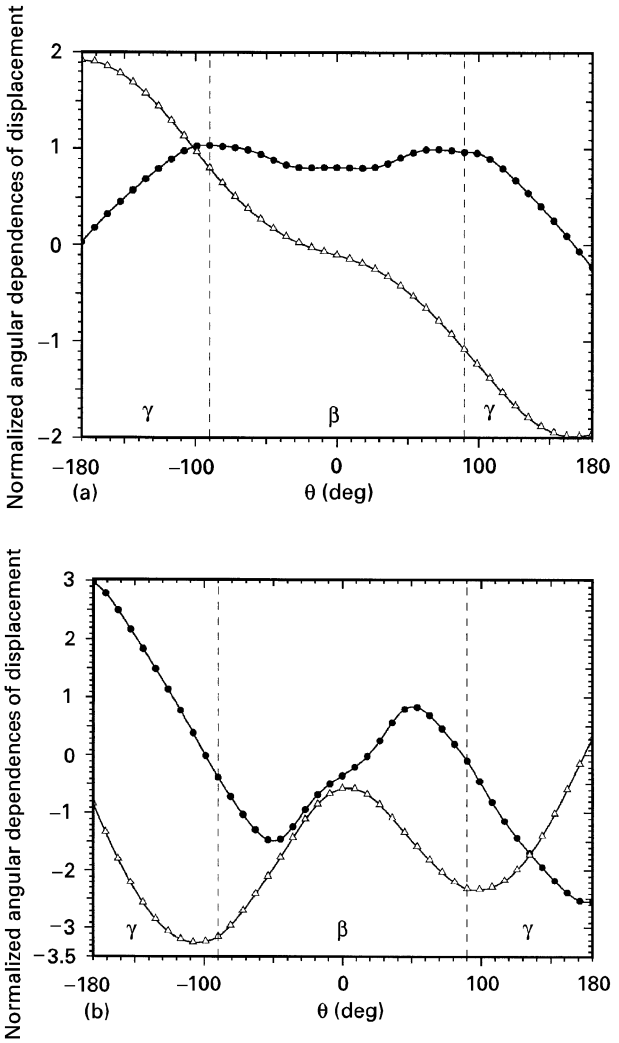

Figure 4 Displacement fields for the γ-TiAl–β-Ti–V case: (a) model A, A = 0.4788, angular dependence of displacement normalized with respect to $h_{\theta\theta}$ (θ = 0); and (b) mode B, B = 0.4113, angular dependence of displacement normalized with respect to $h_{r\theta}$ (θ = 0): (●) u_r, (○) u_θ.

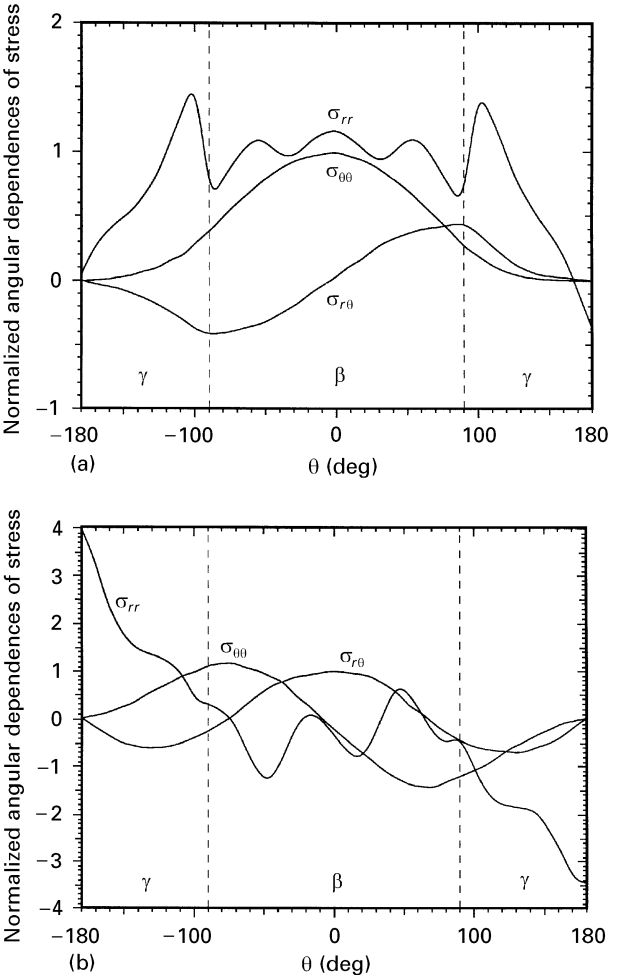

Figure 5 Singular stress fields for the γ-TiAl–β-Ti–V case: (a) mode A, $\lambda_A = 0.4788$, angular dependence of displacement normalized with respect to $h_{\theta\theta}$ (θ = 0); and (b) mode B, $\lambda_B = 0.4113$, angular dependence of displacement normalized with respect to $h_{r\theta}$ (θ = 0).

nature of the materials used, the local properties of the materials are not constant over the element and hence the Gaussian quadrature method fails to evaluate the element stiffness matrices exactly.

The results shown in Table I indicate that with a model that is large enough (20 elements or larger), the order of Gaussian quadrature does not significantly affect the results. Therefore, for computational efficiency, all the subsequent calculations were done using five integration points per element.

Fig. 4a and b shows the angular variations of the tangential and the radial displacements associated with the two values of λ. It should be noted that for the pure mode I case, the radial displacement is an even function of θ and the tangential displacement is an odd function of θ. Similarly, for the pure mode II case the tangential displacement is an even function of θ and the radial displacement is an odd function of θ. A brief analysis of the results shown in Fig. 4a and b suggests that the two displacement fields are neither pure mode I nor pure mode II. The displacement field associated with λ = 0.4788, named mode A, is more "mode I like", while the displacement field

associated with $\lambda = 0.4113$, name mode B, is more "mode II like".

The angular dependences of the inplane stresses, σ_{rr}, $\sigma_{r\theta}$ and $\sigma_{\theta\theta}$, for the two modes are shown in Fig. 5a and b. The lack of symmetry in the stress functions relative to $\theta = 0$ further confirms that the two modes at hand are neither pure mode I nor mode II. As discussed earlier, the displacement and the stress data shown in Figs 4 and 5 are known within multiplicative constants, the generalized stress intensity factors. It should be noted that, for convenience, the results shown in Fig. 4 and 5 were scaled in such a way that for the mode A, which is mode I like, $h_{\theta\theta}(\theta = 0) = 1$, and for mode B, which is mode II like, $h_{r\theta}(\theta = 0) = 1$, Evaluation of the stress intensity factors is presented in the next section.

2.2. Enriched finite element computation of generalized stress intensity factors

2.2.1. General considerations

To include the effect of the stress singularity at the crack tip into the finite element computation of the generalized stress intensity factors for the case of a crack touching an interface, the region around the crack tip should be analysed using the so called "enriched" quadrilateral elements as initially proposed by Benzley [23]. The effect of the stress singularity at the crack tip is included into the enriched elements by adding to the standard quadratic element displacement interpolation functions the terms that give the proper singularity at the node, which coincide with the crack tip as follows

$$u(\xi, \eta) = \alpha_1 + \alpha_2\xi + \alpha_3\eta + \alpha_4\xi^2 + \alpha_5\xi\eta + \alpha_6\eta^2 + \alpha_7\xi^2\eta + \alpha_8\xi\eta^2 + K_A F_{Au}(\varrho, \theta) + K_B F_{Bu}(\varrho, \theta) \quad (28)$$

and $v(\xi, \eta)$ can be expressed using an analogous equation, where $u(\xi, \eta)$ and $v(\xi, \eta)$ are the x- and y-components of the displacement with the element, and ξ and η are the natural element co-ordinates.

Eight α coefficients in Equation 28, can be determined by evaluating this equation at each of the eight nodes of a given quadratic quadrilateral element. This procedure yields a system of eight linear algebraic equations with eight (α) unknowns in terms of the corresponding eight nodal displacements (u_i or v_i) and the two generalized stress intensity factors, K_A and K_B. After solving this system of equations for α and substituting α into Equation 28 one obtains the following expressions for the inplane displacements, (u, v)

$$u(\xi, \eta) = \sum_{i=1}^{m} N_i(\xi, \eta)u_i + K_A Z(\xi, \eta)\left[F_{Au}(\xi, \eta) - \sum_{j=1}^{m} N_j(\xi, \eta)F_{Auj}\right] + K_B Z(\xi, \eta)\left[F_{Bu}(\xi, \eta) - \sum_{j=1}^{m} N_j(\xi, \eta)F_{Buj}\right] \quad (29)$$

$$v(\xi, \eta) = \sum_{i=1}^{m} N_i(\xi, \eta)v_i + K_A Z(\xi, \eta)\left[F_{Av}(\xi, \eta) - \sum_{j=1}^{m} N_j(\xi, \eta)F_{Avj}\right] + K_B Z(\xi, \eta)\left[F_{Bv}(\xi, \eta) - \sum_{j=1}^{m} N_j(\xi, \eta)F_{Bvj}\right] \quad (30)$$

where N_i are the usual quadratic polynomial interpolation functions expressed in terms of the natural element co-ordinates, ξ and η, and the summation is taken over all m nodes of a given element. For isoparametric quadratic quadrilateral elements used in the present case $m = 8$. The "zeroing" function $Z(\xi, \eta)$ is added in Equations 29 and 30 to obtain the required compatibility between the enriched elements surrounding the crack tip and the regular elements surrounding the enriched elements. This function is equal to unity for the enriched elements, and zero for the regular elements. To obtain the necessary interelement compatibility between the enriched and the regular elements, "transition" elements had to be introduced in which the zeroing function, $Z(\xi, \eta)$, varied between one and zero. Any zeroing function used must be unity along the boundaries of the transition elements that are in contact with the enriched elements and zero on the edges of the elements that are in contact with the regular elements. The specific choice of $Z(\xi, \eta)$ for a given transition element depends on whether an entire edge or a single corner node of the transition element is in contact with the enriched elements surrounding the crack tip. In the present work the following form of $Z(\xi, \eta)$ was used [7, 8]

$$Z(\xi, \eta) = \begin{cases} \frac{1}{4}(1 \pm \xi)(1 \pm \eta): & \text{zeroing from corner node} \\ \frac{1}{2}(1 \pm \xi): & \text{zeroing from element edge} \\ \frac{1}{2}(1 \pm \eta): & \text{zeroing from element edge} \end{cases} \quad (31)$$

Functions F_{Au}, F_{Av}, F_{Bu} and F_{Bv} in Equations 29 and 30 are the coefficients of the stress intensity factors K_A and K_B in the expressions for the x- and y-components of the singular displacement field. In other words

$$\begin{aligned} F_{Au}(r, \theta) &= r^{\lambda_A}[f_{Ar}(\theta)\cos(\theta) - f_{A\theta}(\theta)\sin(\theta)] \\ F_{Bu}(r, \theta) &= r^{\lambda_B}[f_{Br}(\theta)\cos(\theta) - f_{B\theta}(\theta)\sin(\theta)] \\ F_{Av}(r, \theta) &= r^{\lambda_A}[f_{Ar}(\theta)\sin(\theta) + f_{A\theta}(\theta)\cos(\theta)] \\ F_{Bv}(r, \theta) &= r^{\lambda_B}[f_{Br}(\theta)\sin(\theta) + f_{B\theta}(\theta)\cos(\theta)] \end{aligned} \quad (32)$$

F_{Auj}, F_{Avj}, F_{Buj} and F_{Bvj} are the asymptotic displacement functions given in Equation 32 evaluated at the jth node.

Using the relations $r = (x^2 + y^2)^{1/2}$ and $\theta = \tan^{-1}(y/x)$, functions F_{Au}, F_{Av}, F_{Bu} and F_{Bv} can be expressed in terms of the Cartesian co-ordinates x and y. For the isoparametric elements used here the

co-ordinates of a point inside the element are given in terms of the nodal co-ordinates x_i and y_i as

$$x = \sum_{i=1}^{m} N_i(\xi, \eta) x_i \tag{33}$$

$$y = \sum_{i=1}^{m} N_i(\xi, \eta) y_i \tag{34}$$

Using Equations 33 and 34, functions F_{Au}, F_{Av}, F_{Bu} and F_{Bv} can be expressed in terms of the natural co-ordinates ξ and η.

A careful analysis of Equations 29 and 30 shows that in order to determine the total displacement field in each of the elements around the crack field one must evaluate $2m$ nodal displacements (u_i, v_i; $i = 1, \ldots, m$) and two stress intensity factors K_A and K_B.

For the plane strain condition, the strain components of the element are obtained by differentiating Equations 29 and 30 as follows

$$\varepsilon_x = \frac{\partial u(\xi, \eta)}{\partial x} = \frac{\partial u(\xi, \eta)}{\partial \xi}\frac{\partial \xi}{\partial x} + \frac{\partial u(\xi, \eta)}{\partial \eta}\frac{\partial \eta}{\partial x}$$

$$\varepsilon_y = \frac{\partial v(\xi, \eta)}{\partial y} = \frac{\partial v(\xi, \eta)}{\partial \xi}\frac{\partial \xi}{\partial y} + \frac{\partial v(\xi, \eta)}{\partial \eta}\frac{\partial \eta}{\partial y}$$

$$\gamma_{xy} = \frac{\partial u(\xi, \eta)}{\partial y} + \frac{\partial v(\xi, \eta)}{\partial x}$$

$$= \frac{\partial u(\xi, \eta)}{\partial \xi}\frac{\partial \xi}{\partial y} + \frac{\partial u(\xi, \eta)}{\partial \eta}\frac{\partial \xi}{\partial y} + \frac{\partial v(\xi, \eta)}{\partial \xi}\frac{\partial \xi}{\partial x} + \frac{\partial v(\xi, \eta)}{\partial \eta}\frac{\partial \eta}{\partial x} \tag{35}$$

Using the matrix notation, the element's strain components given in Equation 35 can be expressed as

$$\{\varepsilon\} = [\bar{B}]\{b\} \tag{36}$$

where

$$\{\varepsilon\}^T = \{\varepsilon_x \varepsilon_y \gamma_{xy}\}$$

$$\{b\}^T = \{u_1 v_1 u_2 v_2, \ldots, u_m v_m K_A K_B\}$$

and $[\bar{B}]$ is of the order of $[3 \times (2m + 2)]$ and its elements are comprised of the partial derivatives appearing on the right-hand side of Equation 35.

The partial derivations indicated in Equation 35 can be determined following the standard chain rule for partial differentiation of a function, $\phi(\xi, \eta)$

$$\begin{Bmatrix} \dfrac{\partial \phi(\xi, \eta)}{\partial \xi} \\ \dfrac{\partial \phi(\xi, \eta)}{\partial \eta} \end{Bmatrix} = \begin{bmatrix} \dfrac{\partial x}{\partial \xi} & \dfrac{\partial y}{\partial \xi} \\ \dfrac{\partial x}{\partial \eta} & \dfrac{\partial y}{\partial \eta} \end{bmatrix} \begin{bmatrix} \dfrac{\partial \phi(\xi, \eta)}{\partial x} \\ \dfrac{\partial \phi(\xi, \eta)}{\partial y} \end{bmatrix}$$

$$= [J] \begin{bmatrix} \dfrac{\partial \phi(\xi, \eta)}{\partial x} \\ \dfrac{\partial \phi(\xi, \eta)}{\partial y} \end{bmatrix} \tag{37}$$

Equation 37 can next be inverted to yield

Based on Equations 33 and 34 the Jacobian matrix, $[J]$, can be written as

From Equations 35, 36, 38 and 39, it is evident that matrix $[\bar{B}]$ can be expressed in terms of

$$\begin{bmatrix} \dfrac{\partial \phi(\xi, \eta)}{\partial x} \\ \dfrac{\partial \phi(\xi, \eta)}{\partial y} \end{bmatrix} = [J]^{-1} \begin{Bmatrix} \dfrac{\partial \phi(\xi, \eta)}{\partial \xi} \\ \dfrac{\partial \phi(\xi, \eta)}{\partial \eta} \end{Bmatrix} \tag{38}$$

$$[J] = \begin{bmatrix} \dfrac{\partial N_1}{\partial \xi} & \dfrac{\partial N_2}{\partial \xi} & \cdots & \dfrac{\partial N_m}{\partial \xi} \\ \dfrac{\partial N_1}{\partial \eta} & \dfrac{\partial N_2}{\partial \eta} & \cdots & \dfrac{\partial N_m}{\partial \eta} \end{bmatrix} \begin{bmatrix} x_1 & y_1 \\ x_2 & y_2 \\ \vdots & \vdots \\ x_m & y_m \end{bmatrix} \tag{39}$$

the natural co-ordinates ξ and η alone. Matrix $[\bar{B}]$ along with the material's constitutive relation, $\{\sigma\} = [D]\{\varepsilon\}$, can next be used in the standard virtual work expression analogous to the one given in Equation 9, to determine the enriched (transition) element stiffness matrix, $[k]$,

$$[k] = \int_{\Omega} \bar{B}^T [D][\bar{B}]\, d\Omega = \int_{-1}^{1}\int_{-1}^{1} \bar{B}^T [D][\bar{B}] \det[J]\, t\, d\xi\, d\eta \tag{40}$$

where Ω and t are, respectively the element volume and thickness. Based on Equation 36, it can be seen that $[k]$ is a $[(2m + 2) \times (2m + 2)]$ square matrix that has the following form

$$[k] \begin{bmatrix} [k^{11}] & \vdots & [k^{12}] \\ (2m \times 2m) & \vdots & (2m \times 2) \\ \cdots\cdots\cdots & \vdots & \cdots\cdots\cdots \\ [k^{21}] & \vdots & [k^{22}] \\ (2 \times 2m) & \vdots & (2 \times 2) \end{bmatrix} \tag{41}$$

where matrix $[k^{11}]$ is identical to the stiffness matrix for a regular quadratic quadrilateral element, $[k^{12}] = [k^{21}]^T$ contains the contribution of both the regular and the enriched parts of Equations 29 and 30, and $[k^{22}]$ contains only the contribution of the enriched parts of Equations 29 and 30.

The integration indicated in Equation 40 can be done using the Gaussian quadrature procedure

$$[k] = \sum_{I=1}^{NPQ}\sum_{J=1}^{NPQ} F(\xi_I, \eta_J) W_I W_J \tag{42}$$

where NPQ is the number of Gaussian integration points; $F(\xi, \eta) = [\bar{B}]^T [D][\bar{B}] \det[J]\, t$ is the integrand in Equation 40; ξ_I, η_I and W_I, W_J are the Gaussian points and the corresponding weighting factors. It should be noted that because of strain singularity at the crack tip, to compute the stiffness matrix of the enriched elements accurately a higher order integration (large NPQ) is required. For the γ–β case analysed in the next section, we found that the convergence of the solution was met for $NPQ \geqslant 16$. Equation 42 can then be used to evaluate the stiffness matrix for each element, enriched, transition or regular, in the model. Once the element's stiffness matrices are determined they can be assembled into a global stiffness matrix of the system being analysed. Solution of

the global finite problem then yields the values for the unknowns in the system, that is the nodal displacements, u_1, v_1, ..., and the two generalized stress intensity factors, K_A and K_B.

2.2.2. Application to the γ-TiAl–β-Ti–V system

Before proceeding with the calculation of the generalized stress intensity factors, K_A and K_B, the problem of a crack in the γ-TiAl matrix impinging on a β-phase particle, Fig. 1a, is first reduced to a simpler case of a layered γ–β composite with broken laminates of the γ-phase under constant remote displacement loading in the y-direction as shown in Fig. 6a. One may argue that the two configurations, the one shown in Fig. 1a and the one shown in Fig. 6a, are quite different. While this may be the case, our main objective here was to assess, in a time-efficient fashion, the approximate range of the relative contributions of the two singular terms. The geometry of the specimen and the loading conditions used in the finite element analysis are shown in Fig. 6b. To assess the effect of the specimen geometry on the relative magnitude of the generalized stress intensity factors, the width, w, and the length, l, of the specimen were varied relative to the sizes of the enriched–transition regions, d, as indicated in Table II.

The entire computational region was divided into 4500 quadrilateral elements of the same size. Four sizes of the enriched–transition regions, d, were investigated: (a) the region containing four enriched and 12 transition elements, (b) 16 enriched and 20 transition elements, (c) 36 enriched and 28 transition elements, and (d) 64 enriched and 36 transition elements. The remaining elements in the model were the standard quadratic quadrilateral elements. The assembly and the solution of the present enriched element problem was done using the general purpose finite element code ABAQUS [24]. ABAQUS allows the user through a USER ELEMENT option to specify the stiffness matrix of each of the enriched and the transition elements used.

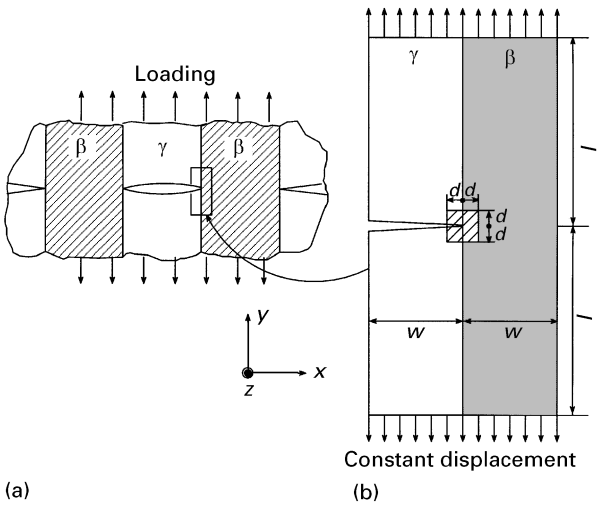

Figure 6 Geometry and schematic of the finite element model used to determine the generalized stress intensity factors for the γ-TiAl–β-Ti–V case.

TABLE II The effect of the specimen geometry on the magnitude of the generalized stress intensity factors

	Case a	Case b	Case c	Case d
w/d	30/2	30/4	30/6	30/8
l/d	150/2	150/4	150/6	150/8
K_A, MPa $\mu m^{0.47885}$	1.970	1.980	1.990	1.990
K_B, MPa $\mu m^{0.41138}$	0.170	0.180	0.180	0.180
K_B/K_A, $\mu m^{-0.06747}$	0.086	0.091	0.094	0.094

The results obtained for the four sizes of the enriched–transition zones are summarized in Table II. These results reveal at least three main features of the problem at hand:

1. There is strong coupling between the two singular terms: i.e. even though only mode I loading was applied, both mode I like, mode A, and mode II like, mode B, stress and displacement fields are activated. This finding is in sharp contrast to the case of a crack touching the interface of two isotropic materials where the two modes, mode I and mode II, are completely decoupled and mode I loading gives rise only to mode I singular stress and displacement fields [25].

2. For the specimen geometry used, the extent of coupling is not significantly affected by the dimensions of the specimen Table II. This finding is apparently related to the results in Table I that show two distinct values for the orders of stress singularity, in sharp contrast to the case of a crack touching the interface of two isotropic materials where one finds a double root for the order of stress singularity, i.e. $\lambda_1 = \lambda_2$.

3. For the given specimen geometry, $l/d = 5$, convergence of the calculated generalized stress intensity factors is achieved when the sizes of the enriched–transition regions are larger than approximately $d = 6w/30$.

The results for K_A and K_B from Table II, along with the stress singularity data, Table I, and the angular dependence functions shown in Figs 4 and 5 and Equations 1 and 2 will be used in Part 2 of this paper [24], to prescribe the displacement and/or stress boundary conditions in the atomistic simulation study of crack tip martensitic transformation in the γ-TiAl–β-Ti–V system.

3. Conclusions

The main findings obtained in the present work can be summarized as follows. The singular stress field associated with a crack touching the interface between two anisotropic materials, such as γ-TiAl and β-Ti–V, contains two terms. The terms have distinct orders of stress singularity. In general, the stress and displacement fields have a lack of symmetry so that they have neither pure mode I nor pure mode II characters. Lastly, the two terms are coupled and each make significant contributions to the singular stress and displacement fields even under simple loading conditions, such as uniaxial mode I loading.

Acknowledgements

The work presented here has been supported by the National Science Foundation under Grants DMR-9317804 and CMS-9531930. The authors are indebted to Drs Bruce A. MacDonald and William A. Spitzig of NSF for their continuing interest in the present work. Helpful discussions with Professors P. F. Joseph and S. B. Biggers, Dr S. S. Pageau, Mr K. Gadi, Mr. N. Zhang and Mr J. Du are greatly appreciated.

References

1. S. C. HUANG and E. L. HALL, in MRS Symp. Proc. **48** (1988) 693.
2. E. M. SCHULSON, *MRS Symp. Proc.* **39** (1985) 193.
3. P. DANG, PhD thesis, Clemson University, August 1996.
4. G. B. OLSON and M. COHEN, in "Mechanical properties and phase transformations in engineering materials", edited by S. D. Antulovich, R. O. Ritchie and W. W. Gerberich (TMS, American Institute of Mining, Metallurgy and Petroleum Engineers, Warendale, PA, 1986) p. 367.
5. I.-W. CHEN, *J. Amer. Ceram. Soc.* **69** (1986) 189.
6. C. L. HOM and R. M. MCMEEKING, *Int. J. Solids Struct.* **26** (1990) 1211.
7. A. R. ZAK and M. L. WILLIAMS, *J. Appl. Mech.* **30** (1963) 142.
8. D. B. BOGGY, *ibid.* **38** (1971) 911.
9. J. COOK and F. ERDOGAN, *Int. J. Engng Sci.* **10** (1972) 677.
10. D. N. FENNER, *Int. J. Fracture* **12** (1976) 705.
11. S. S. PAGEAU, P. F. JOSEPH and S. B. BIGGERS Jr, *Int. J. Solids Struct.* **32** (1995) 571.
12. *Idem*, *Int. J. Numerical Methods in Eng.* **38** (1995) 81.
13. W. K. LIM and C. S. LEE, *Engng Fracture Mech.* **52** (1995) 65.
14. K. S. GADI, P. F. JOSEPH and A. C. KAYA, in Proceedings of the American Society for Mechanical Engineers, Materials Division, MD-Vol. 69-1, (IMECE, 1995).
15. J. S. RAJU and J. H. CREWS, *Computers Structures* **14** (1981) 21.
16. R. S. BARSOUM, *Int. J. Numerical Methods in Engng* **26** (1988) 531.
17. Z. P. BAZANT and L. F. ESTENSSORO, *Int. J. Solids Structures* **13** (1977) 479.
18. Y. YAMADA and H. OKUMURA, in "Hybrid and mixed finite methods", edited by S. N. Atluri, E. R. Gallagher and O. C. Zienkiewicz (Wiley, New York, 1983) p. 325.
19. J. P. BENTHEM, *Int. J. Solids Structures* **13** (1977) 479.
20. D. MUNZ and Y. Y. YANG, *ASME J. Appl. Mech.* **59** (1992) 857.
21. Y. YAMADA and H. OKUMURA, in Proceedings of the Japan–USA Conference, edited by K. Kawata and T. Akasaka, Tokyo (1981) pp. 55–64.
22. M. GRUJICIC and P. DANG, *J. Mater. Sci.* **32** (1997).
23. S. BENZLEY, *Int. J. Numerical Methods in Engng* **8** (1974) 537.
24. ABAQUS Computer Program, Version 5.4, Hibbit, Karlsson & Sorensen, Inc., Providence, RI, September (1995).
25. K. S. GADI, P. F. JOSEPH and A. C. KAYA, in Durability and damage tolerance of composites symposium", International Mechanical Engineering Congree and Exposition, 12–17 November, San Francisco, CA 1995

Received 19 April 1996
and accepted 2 April 1997